

See discussions, stats, and author profiles for this publication at: <https://www.researchgate.net/publication/263939207>

# Optimized Synthesis of CdTe Nanoplatelets and Photoresponse of CdTe Nanoplatelets Films

ARTICLE *in* CHEMISTRY OF MATERIALS · JUNE 2013

Impact Factor: 8.35 · DOI: 10.1021/cm4006844

---

CITATIONS

17

---

READS

39

## 8 AUTHORS, INCLUDING:



Brice Nadal

Nexdot

26 PUBLICATIONS 283 CITATIONS

[SEE PROFILE](#)



Emmanuel Lhuillier

Pierre and Marie Curie University - Paris 6

48 PUBLICATIONS 294 CITATIONS

[SEE PROFILE](#)



Benjamin Abecassis

French National Centre for Scientific Research

30 PUBLICATIONS 599 CITATIONS

[SEE PROFILE](#)



Xiangzhen Xu

École Supérieure de Physique et de Chimie In...

29 PUBLICATIONS 249 CITATIONS

[SEE PROFILE](#)

# Optimized Synthesis of CdTe Nanoplatelets and Photoresponse of CdTe Nanoplatelets Films

Silvia Pedetti,<sup>†</sup> Brice Nadal,<sup>†</sup> Emmanuel Lhuillier,<sup>†</sup> Benoit Mahler,<sup>†</sup> Cécile Bouet,<sup>†</sup> Benjamin Abécassis,<sup>‡</sup> Xiangzhen Xu,<sup>†</sup> and Benoit Dubertret<sup>\*,†</sup>

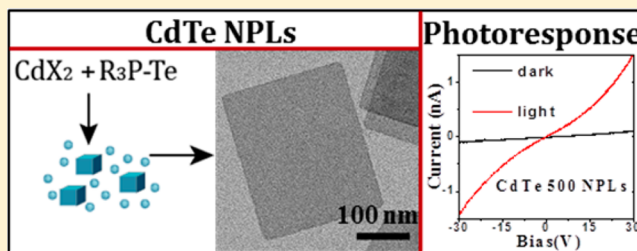
<sup>†</sup>Laboratoire de Physique et d'Etude des Matériaux, CNRS, UMR 8213 ESPCI, 10 rue Vauquelin, 75005 Paris, France

<sup>‡</sup>Laboratoire de Physique des Solides, Univ. Paris-Sud, CNRS, UMR 8502, 91405 Orsay, France

## Supporting Information

**ABSTRACT:** We study in detail the synthesis of CdTe nanoplatelets. Three populations of nanoplatelets with a thickness defined with atomic precision are obtained. We show that CdTe nanoplatelets can be extended laterally to obtain nanosheets with lateral dimensions in the micrometer range. We present the study of the reaction conditions for the formation of CdTe nanoplatelets and for their lateral extension. The reaction products are analyzed with optical spectroscopy, transmission electron microscopy, and small-angle X-ray scattering. We investigate the electro-optical properties of films formed with CdTe nanoplatelets, and we show that their current photoresponse is better than the one of comparable films formed with CdTe spherical nanocrystals.

**KEYWORDS:** CdTe, 2D system, nanoplatelets, current photoresponse



## INTRODUCTION

Since the seminal work of Henglein<sup>1</sup> and Ekimov<sup>2</sup> and the first organometallic synthesis of highly monodisperse semiconductor nanocrystals (NCs),<sup>3</sup> the synthesis of colloidal nanocrystals has constantly improved. These improvements include the realization of core/shell<sup>4</sup> structures, the extension to various materials,<sup>5</sup> as well as a better understanding of the NCs formation mechanisms.<sup>6</sup> The control of the morphology<sup>7</sup> of the nanocrystals is more recent. First synthesized with spherical shapes, the NCs were later synthesized as nanorods,<sup>8</sup> nanowires,<sup>9</sup> and nanoparticles with two-dimensional (2D) morphologies such as nanoribbons<sup>10</sup> or nanoplatelets.<sup>11</sup>

The interest for objects with 2D geometry is motivated by their exceptional electrical,<sup>12</sup> optical,<sup>13</sup> and mechanical<sup>14</sup> properties. Among these materials, colloidal II–VI semiconductors, such as CdSe nanoplatelets (NPLs), hold a special place because they are the first colloidal NPLs that have been synthesized with a control of their thickness with atomic precision.<sup>11</sup> This results in optical and electrical properties very close to the ones observed in epitaxially grown quantum wells.<sup>13</sup>

CdSe 2D nanocrystals have been synthesized in two different crystal structures. In the wurtzite crystal phase, nanoribbons,<sup>10</sup> nanosheets,<sup>15</sup> and quantum belts<sup>16</sup> have been obtained. Although they have different names, these objects are very similar in composition, optical properties, and crystalline structure as well as in their formation mechanism that is based on soft molding of small CdSe clusters.<sup>15,17</sup> CdSe 2D nanocrystals have also been synthesized in a zinc-blende crystal

structure and have been coined nanoplatelets,<sup>11</sup> or quantum disks.<sup>18</sup> Their cubic crystal structure results in NPLs with important differences compared to their wurtzite counterpart. First, their large 2D facets are composed of cationic planes, that facilitate the synthesis of core/shell NPLs, as recently reported.<sup>19</sup> Second, their formation mechanism proceeds through lateral extension of small seeds by continuous precursor reaction.<sup>20</sup> As a result, NPLs with various lateral sizes from small (10 nm) and free floating in solution to large (700 nm) can be synthesized.<sup>21</sup> This pioneer work on CdSe colloidal 2D systems has later been extended in detail to CdS<sup>13,22</sup> but only briefly to CdTe.<sup>13,15</sup>

However, CdTe, with its low band gap ( $E_g = 1.44$  eV),<sup>23</sup> is a very interesting material for photovoltaic<sup>24</sup> and photodetection<sup>25</sup> applications. As a result, many methods to synthesize CdTe colloidal nanocrystals have been reported over the past years.<sup>26</sup> These include organometallic<sup>27</sup> and aqueous routes<sup>28</sup> for the synthesis of spherical NCs on a wide range of size, CdTe nanorods,<sup>29</sup> nanowires,<sup>30</sup> and nanotubes.<sup>31</sup> On the other hand, there are few reports on the colloidal synthesis of 2D CdTe semiconductors. The self-assembly of CdTe nanoparticles with tetrahedral shape in free-floating sheets<sup>32</sup> has been reported, and the synthesis of wurtzite CdTe nanoribbons has been mentioned.<sup>15</sup> The synthesis of zinc-blende CdTe NPLs and the modeling of their electronic transitions have

Received: February 28, 2013

Revised: April 30, 2013

Published: May 21, 2013

been reported,<sup>13</sup> but the synthesis protocols have not been optimized so that mixtures of several NPLs populations with limited lateral dimensions were obtained. In addition, the reaction mixtures contained several byproducts such as large CdTe aggregates.

In this paper, we report a detailed study of the synthesis of colloidal CdTe NPLs. We describe the synthesis of three families of NPLs with different thicknesses that will be referred to by the wavelength value of their first excitonic peak: 428 NPLs, 500 NPLs, and 556 NPLs. Care has been devoted to the control of the size, the shape, and the purity (i.e., only one population per batch) of the CdTe NPLs. The influence of various parameters, such as the nature of the cadmium precursor, of the ligands and the injection rate were investigated. The effect of the injection temperature of the tellurium precursor was also studied. Small angle X-ray scattering (SAXS) experiments elucidate the organization of NPLs in solution and confirm the difference of one monolayer between two successive families of NPLs. We propose a mechanism for the formation of CdTe NPLs on the basis of kinetic studies. Finally, we discuss the electro-optical properties of these CdTe NPLs with in mind the use of these nanoplatelets for optoelectronic devices.

## ■ EXPERIMENTAL SECTION

**Chemicals.** Cadmium acetate dihydrate  $\text{Cd}(\text{OAc})_2 \cdot 2(\text{H}_2\text{O})$  (Sigma-Aldrich, 98%), oleic acid (OA, Sigma-Aldrich, 90%), 1-octadecene (ODE, Sigma-Aldrich, 90%), trioctylphosphine (TOP, Cytec, 90%), tellurium (Sigma-Aldrich, 99.997%), propionic acid (Sigma-Aldrich, 99%), CdO (Sigma-Aldrich, 99%), cadmium formate (Sigma-Aldrich, 99.9%), *n*-hexane (VWR, 95%), and ethanol (Carlo Erba, 99.8%) are purchased for the synthesis of the nanoplatelets and used without any further purification.

**Materials Characterization.** Optical absorption and photoluminescence spectroscopy are performed using respectively an UV visible spectrometer (Varian Cary 5E) and photoluminescence spectrometer (Jobin-Yvon Horiba, Fluoromax-3). Transmission electron microscopy (TEM) imaging is done using a JEOL 2010 with a FEG, while X-ray diffractograms are obtained from a Philips X'Pert system with a Cu  $\text{K}\alpha$  source. SAXS measurements were carried out at the SWING beamline of the SOLEIL synchrotron (Saint-Aubin, France). Experiments were performed using a fixed energy of 12 keV and three sample to detector positions (0.85, 1.07, 6.56 m). The typical accessible range of scattering vector modulus  $q$  was  $0.01 - 1 \text{ \AA}^{-1}$  ( $q = 4\pi \sin \theta/\lambda$ , where  $2\theta$  is the scattering angle and  $\lambda = 0.033 \text{ \AA}$  the wavelength). Scattering patterns were recorded on an AVIEX 170170 CCD camera formed by four detectors and radially averaged. SAXS experiments were performed on precipitate of NPLs transferred in a glass capillary. After the synthesis, the nanoparticles are dispersed in hexane. Due to their large lateral extension, van der Waals forces tend to provoke the flocculation of the platelets in solution. This yields, after a few hours at rest, a concentrated "wet" precipitate used for the measurement.

**Precursors Synthesis.** The cadmium propionate ( $\text{Cd}(\text{prop})_2$ ) is made using the followings steps: 1.036 g of CdO (8.07 mmol) and 10 mL of propionic acid are charged into a flask. The mixture is heated at 70 °C for 1 h under argon. When the entire solid is dissolved and a colorless solution is obtained, the heating is stopped and acetone is added to precipitate the product as a white solid. Then it is filtered off, washed with acetone, and dried under vacuum overnight.

**Nanoplatelets Synthesis. Synthesis of CdTe 428 NPLs.** A three-neck flask is charged with 130 mg of  $\text{Cd}(\text{prop})_2$  (0.5 mmol), 80  $\mu\text{L}$  of OA (0.25 mmol), and 10 mL of ODE, and the mixture is magnetically stirred and degassed under vacuum at 95 °C for 2 h. The mixture under argon is heated at 180 °C and 100  $\mu\text{L}$  of a solution of 1 M TOP-Te diluted in 0.5 mL of ODE are swiftly added. The color of the solution changes rapidly and becomes yellow. Aliquots are taken at

different stages of the reaction to follow it spectroscopically. The reaction is performed for 20 min at the same temperature. OA (1 mL) is added to the solution, and the heating mantle is quickly removed. At room temperature, 30 mL of hexane and 40 mL of ethanol are added to the crude reaction mixture. Nanoplatelets are then precipitated through centrifugation for 10 min at 5000 rpm. The supernatant is discarded, and the solid precipitate is redispersed in hexane. The precipitation process is repeated two or three times.

When 428 NPLs are prepared using  $\text{Cd}(\text{OAc})_2$ , TOP-Te 1 M is injected between 120 and 140 °C.

**Synthesis of CdTe 500 NPLs.** A three-neck flask is charged with 130 mg of  $\text{Cd}(\text{prop})_2$  (0.5 mmol), 80  $\mu\text{L}$  of OA (0.25 mmol), and 10 mL of ODE, and the mixture is magnetically stirred and degassed under vacuum at 95 °C for 2 h. The mixture under argon is heated at 210 °C, and 100  $\mu\text{L}$  of a solution of 1 M TOP-Te diluted in 0.5 mL of ODE is swiftly added. The color of the solution changes rapidly to become yellow and then yellow-orange. The reaction is heated for 30 min at the same temperature. Then, 1 mL of OA is added to the solution, and the heating mantle is quickly removed. At room temperature, 30 mL of hexane and 40 mL of ethanol are then added to precipitate the NPLs. The solution is then centrifuged for 10 min at 5000 rpm. The supernatant is discarded and the solid precipitate is redispersed in hexane. The precipitation process with the ethanol is repeated two or three times.

When  $\text{Cd}(\text{OAc})_2$  was used as cadmium precursor, TOP-Te is injected between 170 and 190 °C.

**Synthesis of CdTe 500 NPLs with Continuous Injection.** A mixture of 160 mg  $\text{Cd}(\text{OAc})_2 \cdot 2(\text{H}_2\text{O})$  (0.6 mmol) and 95  $\mu\text{L}$  OA (0.3 mmol) in 25 mL of ODE is charged into a three-neck flask and stirred under vacuum for 1 h at 95 °C. The flask is filled with Ar, and the temperature is increased to 200 °C. Then, 0.1 mmol of stoichiometric TOP-Te (2.24 M) diluted in 5 mL ODE is injected with a syringe pump at a constant rate over 30 min. When the addition is completed, the reaction is heated at 200 °C for 15 min. Hexane (30 mL) and ethanol (30 mL) are added to the crude product, and the NPLs are precipitated by centrifugation at 3500 rpm and then redissolved in hexane or toluene.

**Synthesis of CdTe 556 NPLs.** In a typical reaction, 133 mg of  $\text{Cd}(\text{OAc})_2$  (0.5 mmol), 255  $\mu\text{L}$  of OA (0.8 mmol), and 25 mL of ODE are charged into a three-neck flask, and the mixture is stirred and degassed under vacuum at 95 °C for 2 h. The flask is filled with argon, and the temperature is increased to 215 °C. Then, 0.05 mmol of stoichiometric TOP-Te (2.24 M) diluted in 2.5 mL ODE is injected with a syringe pump at a constant rate over 15 min. When the addition is completed, the reaction is heated for 15 min.

**Films Preparation.** To estimate the absorption coefficient of a film of NPLs, three films of different thicknesses are prepared on a glass substrate. The NPLs initially stored in hexane are precipitated by the addition of ethanol. The mixture is centrifuged, and the precipitate is redispersed in a mixture of hexane and octane (9:1 volume ratio). Glass microscope slides are cleaned by sonication: 15 min in acetone, 15 min in ethanol, and finally, 15 min in 1 M HCl aqueous solution. Once dried under air flow, the slide is dipped into a tetraethyl orthosilicate (TEOS) solution (10 vol % in ethanol) and finally heated using the heat gun. The solution of NPLs is drop-casted onto this slide. Their absorption and their thickness are measured using a profilometer (Fogale Nanotech, Nanosurf 3D optical profilometer).

**Transport Measurements.** For transport measurements, a solution of CdTe 500 NPLs in hexane/octane is drop-casted onto interdigitated electrodes. The latter are gold electrodes on glass substrate and composed of 25 pairs that are 2.5 mm long and spaced at 10  $\mu\text{m}$ . Once the film is dried, it is dipped into a solution of propylamine diluted in ethanol (1 vol %) before being rinsed in pure ethanol.<sup>33</sup> The deposition process is repeated three times to obtain a thickness of a few hundreds of nanometers. *I*–*V* measurements are obtained using a Keithley 2400 electrometer. The *I*–*V* under illumination is performed using a blackbody illuminating the sample at 3000 K. The frequency response of the system under illumination is obtained by biasing the system by a Keithley 2400 as bias source; then, the signal is magnified with a  $10^8$  gain using a current amplifier

(Keithley 427). The illumination is done through a 405 nm laser source modulated by a signal generator (Agilent 33120). The signal is then acquired on the oscilloscope (HP 54600).

## RESULTS AND DISCUSSION

We have developed optimized protocols, detailed in the Experimental Section, for the synthesis of CdTe NPLs (Figure 1) with their first excitonic peak respectively at 428 nm, 500

nm, and 556 nm. These NPLs populations correspond to three different NPLs thicknesses. The protocols we used are based on the injection of TOP-Te at high temperature into a solution composed of a cadmium precursor, oleic acid, and octadecene. These three NPLs populations were characterized in absorption, with transmission electron microscopy (TEM), with powder X-ray diffraction (XRD), and with small angle X-ray scattering (SAXS).

For each population of NPLs, we can recognize on the absorption spectrum a sharp peak that corresponds to the first excitonic transition electron/heavy hole, followed by a broader one for the electron/light hole transition. These two transitions lie at 428 and 386 nm for the 428 NPLs (Figure 1a), at 500 and 448 nm for the 500 NPLs (Figure 1b) and at 556 and 501 nm for the 556 NPLs (Figure 1c). The photoluminescence emission spectra for the first two thinnest NPLs populations show a single emission peak with a narrow full width at half-maximum (fwhm)  $\leq 7$  nm and no detectable Stokes shift. The PL quantum yield remains low (typically in the 0.1 to 1% range). In the case of the 556 NPLs in Figure 1c, other NPLs populations can be detected in the emission spectrum, but not in the absorption spectrum, and a broad signal present at low energy is characteristic of deep-trap emission.

The X-ray powder diffraction (XRD) of the three populations of CdTe NPLs confirmed a cubic zinc blende structure (Figure S1c in Supporting Information). A TEM image of a single 556 NPL is shown on the Figure S1a (see the Supporting Information). The platelet lies on the top face and the contrast on the surface is homogeneous. The pattern in the Fast Fourier Transform (FFT) picture can be interpreted as {220} reflections (Figure S1b in the Supporting Information). The thickness direction is then parallel to the [001] axis, while the edges of NPLs are found to be perpendicular to [100] or [010] axis. Extension of NPLs during the growth stage occurs along these axes.

We also conducted some SAXS experiments on aggregated CdTe NPLs. This technique is well suited to unravel the large-scale organization of nanocrystals in solution,<sup>34</sup> and it is complementary with TEM, since the scattered intensity is averaged over numerous nanoparticles. In Figure 2a, we reported three characteristic scattering patterns in logarithmic scale obtained for each family of aggregated CdTe nanoplatelets as detailed in the Experimental Section. Each curve presents three Bragg peaks between 0.1 and 1  $\text{\AA}^{-1}$  that we can index as

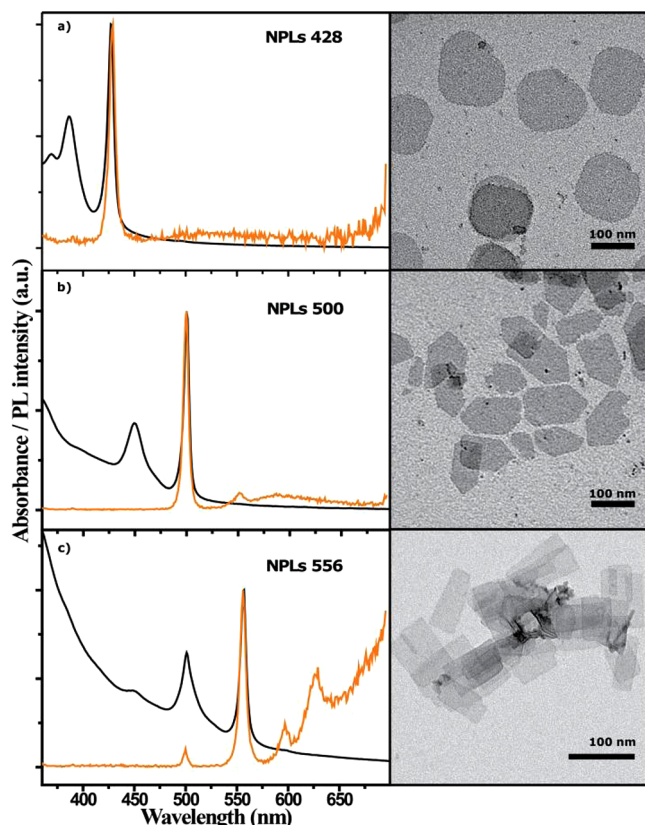


**Figure 1.** CdTe NPLs with three different thicknesses. Left, absorption (black) and photoluminescence (orange) spectra of NPLs with different thicknesses. Right, TEM images of the corresponding samples. (a) NPLs with the first excitonic peak at 428 nm, (b) NPLs with the first excitonic peak at 500 nm, (c) NPLs with the first excitonic peak at 556 nm.

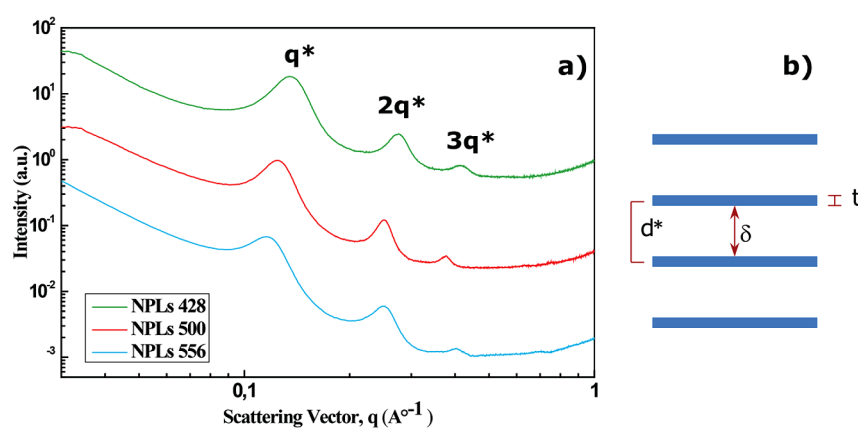


**Figure 2.** SAXS measurements. (a) Characteristic scattering patterns for each NPLs population. For each curve, three Bragg peaks are present:  $q^*$ ,  $2q^*$ ,  $3q^*$ . (b) Schematic illustration of NPLs stacking. Values of  $d^*$  include the NPLs thickness ( $t$ ) and the distance between two NPL edges ( $\delta$ ).

$q^*$ ,  $2q^*$ , and  $3q^*$ . Their presence is due to the one-dimensional lamellar stacking of the NPLs in solution. Qualitatively, we observe that the larger the NPLs, the smaller the  $q^*$ . From the position of the peaks, we can estimate distances values  $d^*$  from the simple formula  $q^* = 2\pi/d^*$ . This yields to  $d^*$  of  $4.7 \pm 0.1$  nm for 428 NPLs,  $5.1 \pm 0.1$  nm for 500 NPLs, and  $5.4 \pm 0.1$  nm for 556 NPLs.  $d^*$  is the sum of the platelet thickness and the edge-to-edge distance (see Figure 2b). Since the ligands are the same in the different populations, we hypothesize that the edge-to-edge distance is identical for the three populations. As a consequence, the different values of  $d^*$  we observe are due to the thickness difference among the 428, the 500, and the 556 NPLs populations. The increment measured between the different families is  $0.3 \pm 0.1$  nm, that is around half the lattice constant of CdTe ( $\sim 0.65$  nm). These results confirm that each CdTe NPLs population has a thickness equal to an integer number of CdTe monolayers. Moreover, the typical thickness for platelets observed by TEM is 1.6 nm (NPL 428), 1.9 nm (NPL 500), and 2.2 nm (NPL 556), while the thickness of a layer of oleic acid is 2.1 nm.<sup>35</sup> Consequently, the sum of the thickness of the NPL added to two monolayers of oleic acid is higher than the SAXS period, pledging for a partial interdigitation of the ligands when the NPLs are stacked.

We have investigated the formation of the CdTe NPLs with various precursors of tellurium and cadmium. For tellurium, we tested TOP-Te and the more reactive tributylphosphine-Te (TBP-Te). TBP-Te gave uncontrolled formation of large aggregated NPLs (Figure S2 in the Supporting Information), so we used TOP-Te for the rest of our experiments. For the cadmium, we explored three different cationic precursors: cadmium formate ( $\text{Cd}(\text{form})_2$ ), cadmium acetate ( $\text{Cd}(\text{OAc})_2$ ), and cadmium propionate ( $\text{Cd}(\text{prop})_2$ ). NPLs could easily be obtained with both  $\text{Cd}(\text{OAc})_2$  and  $\text{Cd}(\text{prop})_2$ , but when  $\text{Cd}(\text{formate})_2$  is used, it leads to the formation of tetrapod-like nanoparticles (Figure S3 of the Supporting Information). We have further analyzed the NPLs with transmission electron microscopy (TEM). For the two thinnest populations, we observed a difference in the NPLs morphology depending on the choice of the cadmium precursor. When  $\text{Cd}(\text{prop})_2$  is used, the 428 NPLs have a disk-like shape with an average diameter size of 145 nm, while the 500 NPLs have an arrow-like shape with an average length of 150 nm and an aspect ratio between 1.5 and 2 (Figures 1a and b). When  $\text{Cd}(\text{OAc})_2$  is used instead, control of the NPLs thickness could be obtained, but the TEM images show NPLs that are more irregular in shape and less extended laterally (Figure S4 of the Supporting Information). For 556 NPLs, we had to use  $\text{Cd}(\text{OAc})_2$  and a slow injection of cadmium precursors. The 556 NPLs appear rectangular on the TEM images with an average lateral size of 35 nm  $\times$  80 nm (Figure 1c).

In the case of the CdS NPLs, it was shown that the NPLs thickness could be controlled to a certain extent by changing the length of the carbon chain of the carboxylic acid used for the synthesis.<sup>22a</sup> We tested a series of carboxylic acids with different lengths of hydrocarbon chains: myristic acid (C14), oleic acid (18:1 *cis*-9), behenic acid (C22), and erucic acid (22:1 *ω*-9). We observed that, for reactions run under similar conditions, the longer ligands favor the formation of thicker NPLs (Figure S5 of the Supporting Information), although NPLs thicker than the 556 NPLs population could not be obtained in pure form. Under our experimental conditions, these other carboxylic ligands produce NCs agglomerates

during the synthesis (Figure S6 on the Supporting Information).

As a consequence, we stick with the oleic acid and explore the influence of its concentration on the CdTe NPLs synthesis. When the ratio of the oleic acid to the short chain carboxylate cadmium is larger than 2:1, only CdTe spherical nanocrystals or aggregates are obtained (Figure S7 in the Supporting Information). We hypothesize that when the oleic acid is in great excess compared to the short chain carboxylate cadmium precursor, all the cadmium salt is complexed with the long oleic acid chain while the short carboxylate chains evaporate during the degassing step. When the oleic acid/Cd precursor ratio was kept <2:1, we observed that the higher the concentration of oleic acid the smaller the lateral dimensions of the final NPLs. For example, the lateral dimensions of 428 NPLs obtained by injection of TOP-Te at 180 °C in a mixture containing 0.25 mmol of oleic acid (Figure 3a) are roughly two times larger

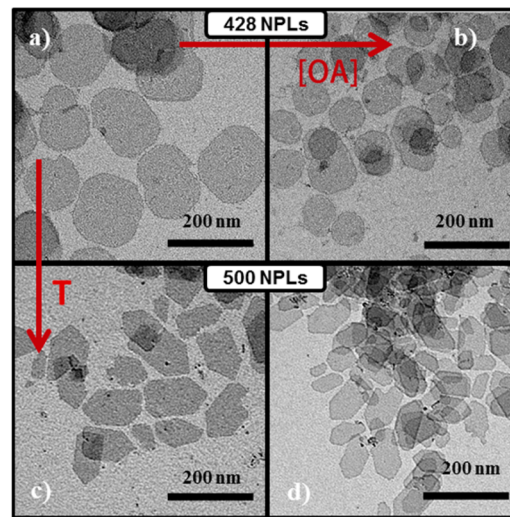


**Figure 3.** Control of the NPLs lateral sizes. TEM images of NPLs synthesized in presence of 0.5 mmol of  $\text{Cd}(\text{prop})_2$  in 10 mL of ODE. The concentration of OA acid is 25 mM in a and c and 50 mM in b and c. 0.1 mmol of TOP-Te 1 M is injected at 180 °C in a and b giving 428 NPLs, while at 210 °C in c and d giving as final product 500 NPLs.

than those obtained when the same synthesis is performed with 0.50 mmol of oleic acid (Figure 3b). Similar behavior is observed when the injection is performed at 210 °C for 500 NPLs (Figure 3c and d).

We now turn to the study of the formation kinetics of the CdTe NPLs, which was explored at different temperatures with two different metallic precursors: cadmium acetate and cadmium propionate. The formation of the NPLs was studied with a measurement of the absorption of constant volumes of the reaction mixture at different moments during the reaction (Figure 4). All reactions were performed by the injection of 100  $\mu\text{L}$  of TOP-Te 1.0 M in 10 mL of ODE mixed with 0.3 mmol of OA and 0.6 mmol of cadmium precursor.

We first studied the kinetic formation of the 428 nm NPLs (Figure 4a). These NPLs are formed as a pure population when TOP-Te is injected at 120 °C. The absorbance at 350 nm, which is proportional to the amount of crystalline CdTe in solution,<sup>36</sup> constantly increases until about 70 min (Figure 4a), and the formation of 428 NPLs is underlined by the appearance of the first excitonic peak at 428 nm whose intensity also

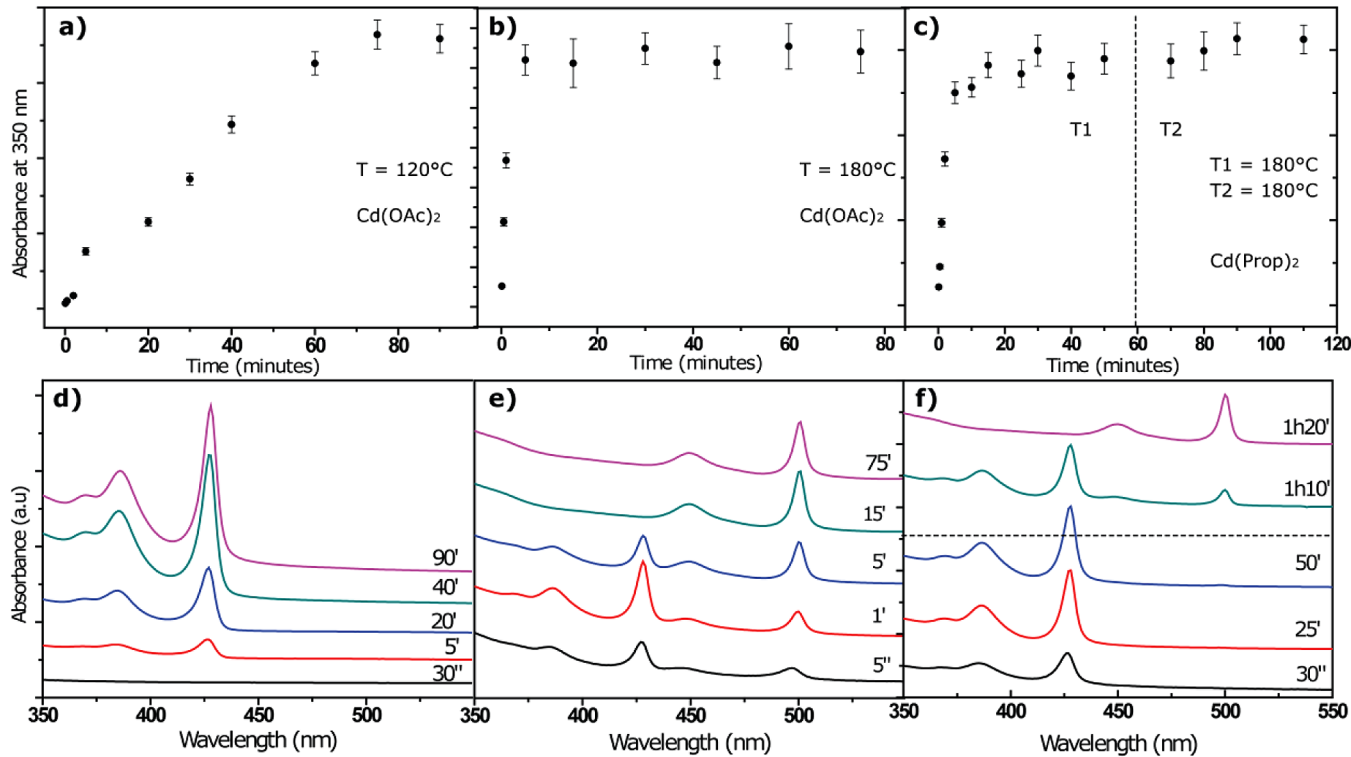
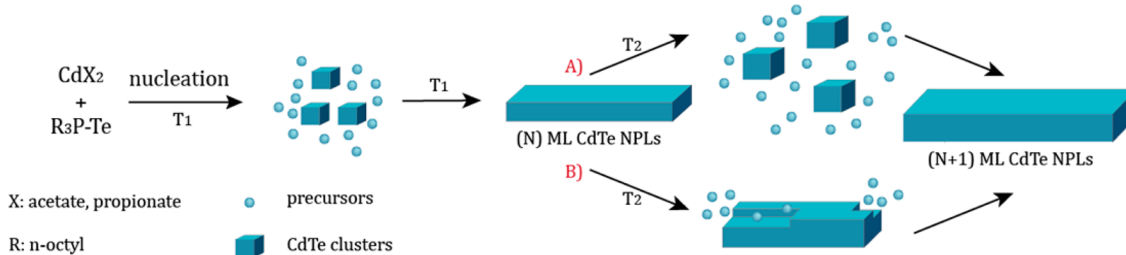


**Figure 4.** Absorption spectra versus time for three different reaction conditions. Top, absorbance at 350 nm after correction due to the sampling (see Supporting Information) when the reaction is performed with (a) Cd(OAc)<sub>2</sub>, at 120 °C, (b) Cd(OAc)<sub>2</sub> at 180 °C, (c) Cd(prop)<sub>2</sub> at 180 °C and then at 210 °C. Bottom, absorption spectra at different times during the reaction.

#### Scheme 1. Possible Mechanistic Schemes to Explain the Thickness Evolution CdTe NPLs during the Synthesis



increases until the end of the reaction (Figure 4d). In these conditions, the thinnest NPLs form gradually and remain stable even after few hours at 120 °C. The same behavior holds when TOP-Te is injected up to 140 °C. However, as the injection (and the reaction) temperature is increased to 150 °C, two populations of NPLs, the 428 NPLs and the 500 NPLs, are formed. They form in different amounts, and the ratio between the two populations is constant over prolonged heating. When the injection is performed at 180 °C, the precursors are consumed after 5 min (Figure 4b) and both the 428 NPLs and the 500 NPLs populations are present even 5 s after the TOP-Te injection (Figure 4e). The thinner population forms faster during the first 5 min, but it gradually disappears to the benefit of the thicker 500 NPLs during the prolonged heating. Once transformed into thicker 500 NPLs, it remains stable until the end of the reaction (75 min). This transformation with heating of NPLs of a given thickness to a thicker population, which differs by just one CdTe monolayer (ML),<sup>13</sup> suggests that the thinnest population dissolves into small parts, which could be clusters, small seeds, or precursors, that reassemble into thicker NPLs that are more stable under these conditions. The

dissolution of the thinnest NPLs did not produce any spherical NCs but only thicker NPLs.

In order to better grasp this dissolution and reassembly process, we explored a third type of reaction conditions (Figures 4c and f). We kept the temperature at 180 °C for the injection, but we replaced the Cd(OAc)<sub>2</sub> with Cd(prop)<sub>2</sub>, which has a slightly longer alkyl chain. During the first part of the reaction, the temperature is fixed at 180 °C (T<sub>1</sub>), which is the injection temperature. An hour after the injection, the reaction temperature is increased to 210 °C (T<sub>2</sub>). After 20 min at 210 °C only NPLs 500 are present in the reaction mixture. During the first part of the reaction, only the thinnest 428 NPLs form and remain stable, even long after the 10 min necessary for the complete formation of crystalline CdTe. The saturation of the absorbance at 350 nm happens at the same time whether Cd(OAc)<sub>2</sub> or Cd(prop)<sub>2</sub> is used, but when Cd(prop)<sub>2</sub> is used, only the 428 NPLs population is formed. Similar instabilities when the temperature increases have been observed in the case of CdS NPLs<sup>22a</sup> with the complete disappearance of a NPLs population at the expense of a thicker one. In the case of CdSe wurtzite quantum belts,<sup>17</sup> this behavior

has also been observed, but no discussion of this evolution has been provided.

It is not clear at this point what precise mechanism yields the dissolution of the thinnest NPLs and the apparition of NPLs with just one more CdTe monolayer. However, two paths can be invoked (Scheme 1). After the nucleation at temperature  $T_1$  of the nanoplatelets seeds, they extend laterally for direct reaction with precursors present in the reaction mixture to form thin NPLs. Subsequently, if  $T_1$  is high enough or if the temperature is increased to  $T_2 > T_1$ , the system composition may change. Either the thinnest NPLs population dissolves completely to furnish 500 NPLs seeds that react rapidly with precursors to give the thicker NPLs that are more stable (Scheme 1, path A) or the thinnest NPLs partially dissolve to favor the growth of a monolayer on existing 428 NPLs for direct reaction with precursors in a sort of ripening mechanism (Scheme 1, path B).

The NPLs we managed to synthesize with a rapid injection of Te precursor had lateral dimensions  $<200$  nm. In the case of CdSe NPLs, it was recently shown that continuous injection of precursors could extend CdSe NPLs to lateral dimension up to 700 nm. We have applied a similar technique to the CdTe NPLs. We injected TOP-Te 2.24 M diluted in ODE into a mixture containing the cadmium precursor and oleic acid in ODE. The choice of TOP-Te saturated was preferred to avoid or minimize the presence of free TOP in the reaction mixture. The injections lasted usually for 30 min, and they were performed at temperatures ranging from 180 to 220 °C.

The absorption spectra taken during the injection (Figure 5) demonstrate the formation of several NPLs populations with a predominance of the 500 NPLs population. Aliquots were sampled from the reaction mixture at various times, purified using precipitation with ethanol and centrifugation, suspended in anhydrous hexane, and observed with TEM. After 2 min (Figure 5a), the NPLs average lateral size is 60 nm, while after 10 min (Figure 5b) it increases up to 120 nm. At 30 min, it reaches on average 500 nm. These results are in agreement with the mechanism already proposed for the growth of CdSe NPLs that suggests the initial formation of some seeds that keep extending through reaction with precursors. Although we cannot completely rule out the secondary nucleation of some NPLs combined to the fact that NPLs laterally extended are extremely fragile, we were able to grow NPLs larger than 800 nm.

In summary, we have shown that the final aspect, shape and thickness of NPLs can be modified and controlled choosing the most suitable conditions for the rate of TOP-Te addition, the ligands concentration, the temperature of injection, and the precursors' ratio. Some examples of CdTe NPLs of different shape and size obtained by tuning the synthetic parameters are listed in Table 1 in the Supporting Information.

Semiconductor NPLs with lateral dimensions close to 500 nm are potentially interesting nanoparticles for the construction of devices such as light emitting diodes,<sup>37</sup> photovoltaic cells,<sup>38</sup> or even photodetectors.<sup>39</sup> We have explored the possibility to assemble the CdTe NPLs into continuous and homogeneous films (see experimental section), and we have measured the photoresponse of these CdTe NPLs films.

The absorption coefficient of a quantum well is given by  $\alpha = (\hbar w e^2 \mu / \hbar^3) (Z_0 / nL) S \phi (r_c \eta)^2$  where  $\hbar$  is the reduced Plank's constant,  $\mu$  the reduced effective mass,  $n$  the optical index of the film,  $Z_0$  the vacuum impedance,  $L$  the thickness of the quantum well,  $S$  the electric field screening factor  $S = ((3\epsilon_{med}) / (2\epsilon_{med}) +$

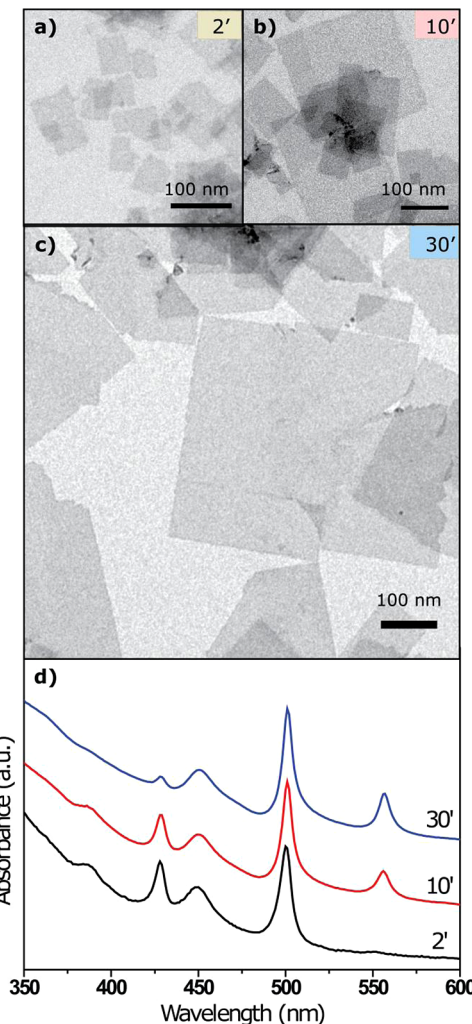


**Figure 5.** Lateral extension of CdTe NPLs. TEM pictures of CdTe NPLs 2 min (a), 10 min (b), and 30 min (c) after the onset of the injection. (d) Corresponding absorption spectra.

$\epsilon_{CdTe}))^2$ ,  $\phi$  the filling factor (0.64 assuming randomly closed packing), which is the fraction of absorbing material into the film taken equal to half,  $\eta$  the polarization term, which for quantum well is  $\eta^2 = 1/2$ , and finally, the dipolar element is related to the Kane energy ( $E_p$ ) through the relation  $r_c = (\hbar / E_G)(E_p / 2m_0)^{1/2}$  with  $E_G$  the bulk band gap and  $m_0$  the free electron mass. All the parameters values are reported in Table S2 in the Supporting Information. The thickness of NPLs with a peak wavelength at 500 nm is  $1.9 \pm 0.3$  nm.<sup>13</sup> This leads to a predicted value of  $2 \pm 0.4 \times 10^4$  cm<sup>-1</sup> for the absorption coefficient, which needs to be compared to the experimental value of  $1.5 \times 10^4$  cm<sup>-1</sup>, see Figure 6a. Most of the uncertainty results from the roughness of the film and the evaluation of the NPL thickness. Moreover, tuning the lateral size within a factor of 5 does not affect the value of the absorption coefficient. At the individual scale, the cross section of an NPL is considerably increased compared to that of a spherical QD,<sup>40</sup> typically by a factor of 100, which corresponds to the change in the particle area. Nevertheless, this advantage is partly washed out once processed under a film form due to the lower density of NPL and the absorption coefficient (integrated over energy) is very similar to the reported value for QD film.

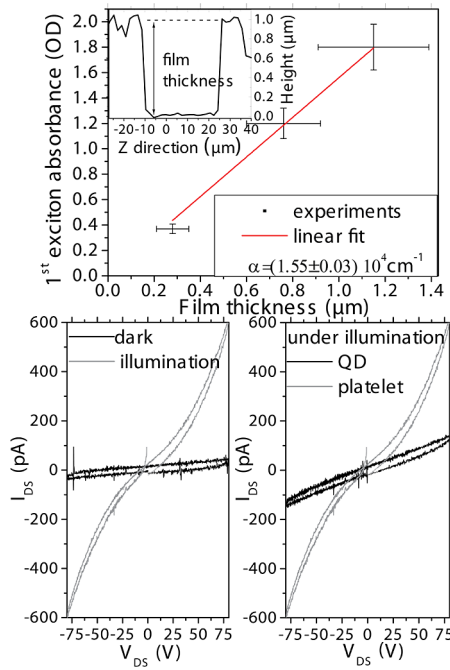


**Figure 6.** (a) Absorbance at the first exciton as a function of the film thickness. Inset: thickness profile of a film of CdTe nanoplatelets. (b)  $I$ – $V$  curves of a film of CdTe 500 NPLs under dark condition and illuminated. (c)  $I$ – $V$  curves under illumination of a film of CdTe 500 NPLs and CdTe QD with an exciton peak at 518 nm. The film thickness is 1  $\mu\text{m}$  in both cases.

As deposited, the material does not show any measurable conductance as long as the NPLs are capped with the initial oleic acid ligand. On the other hand, once ligand exchange<sup>41</sup> with a short amine is performed, we are able to observe a conduction signal. For propylamine capped CdTe NPLs, we measure a resistivity of the order of  $5 \times 10^{11} \Omega\cdot\text{cm}$  under dark condition. Due to the fact that platelets are Cd rich on their surface, the dipping of the film in the short amine solution mostly removed the excess of organic molecules, such as unbound ligands. The film also presents good photoconduction properties as shown in Figure 6b. Comparison of the NPLs with regular 0D CdTe QDs (Figure S11 on Supporting Information), capped with the same ligands is shown in Figure 6c. We typically observe a 4× improvement of the photocurrent signal with the NPLs. This difference can be partly attributed to the size of the object. For colloidal quantum dots film, most of the resistance of the film is due to the tunnel barrier due to the ligands, larger semiconductor nanocrystals consequently reduce the number of hopping step required to reach the electrodes.

The ease to extract the photosignal compared to the dark current tends to indicate that the transport in the film of NPLs is mostly limited by the lack of thermally activated carrier rather than by the carrier mobility. We consequently believe that the CdTe NPLs are a promising material for photoactive optoelectronic applications. Moreover, there is room for a stronger tuning of the film conductivity through alternative ligand exchange strategies<sup>42</sup> and encapsulation in a host high mobility matrix.<sup>43</sup>

## CONCLUSION

We present in this work the synthesis of three populations of CdTe NPLs that were obtained with a high degree of purity in terms of thickness and lateral dimensions. We have investigated

the different parameters of the NPLs synthesis, including various precursors of cadmium and tellurium, various precursors concentrations, and various temperatures both for the precursors injection and for the synthesis. Under optimized conditions, we were able to obtain NPLs with pure thickness, and lateral dimensions that could reach up to 800 nm. NPLs with 500 nm lateral dimensions were tested for optoelectronic devices, and we found that with barely processed material we could easily extract a large photoresponse. In consequence, we believe that CdTe NPLs are a promising material for devices such as photovoltaic cells.

## ASSOCIATED CONTENT

### Supporting Information

(1) FFT pattern and XRD pattern of CdTe NPLs, (2) syntheses using tributylphosphine telluride (TBP-Te) as tellurium precursor, (3) cadmium precursor: Cd(formate)<sub>2</sub>, (4) cadmium precursor: Cd(OAc)<sub>2</sub>, (5) influence of carboxylic acid chain length on the reactivity, (6) carboxylic acids: different chain lengths, (7) OA concentration, (8) absorbance at 350 nm, (9) tuning of shape and size of CdTe NPLs: synthetic parameters, (10) band structure parameters, (11) synthesis of CdTe QDs using diphenylphosphine. This material is available free of charge via the Internet at <http://pubs.acs.org>.

## AUTHOR INFORMATION

### Corresponding Author

\*E-mail: benoit.dubertret@espci.fr.

### Notes

The authors declare no competing financial interest.

## ACKNOWLEDGMENTS

We are grateful to the Soleil Synchrotron (Saint-Aubin, France) for the award of beamtime 20110596. B.D. thanks the ANR, the ESPCI, and the CNRS for funding. We thank Sandrine Ithurria and Mickael Tessier for helpful discussions and Nicolas Lequeux for help with the SAXS measurements.

## REFERENCES

- Henglein, A. *Ber. Bunsen Phys. Chem.* **1982**, 86 (4), 301–305.
- Ekimov, A. I.; Onushchenko, A. A. *JETP Lett.* **1981**, 34 (6), 345–349.
- Murray, C. B.; Norris, D. J.; Bawendi, M. G. *J. Am. Chem. Soc.* **1993**, 115 (19), 8706–8715.
- (a) Hines, M. A.; Guyot-Sionnest, P. *J. Phys. Chem.* **1996**, 100 (2), 468–471. (b) Reiss, P.; Protiere, M.; Li, L. *Small* **2009**, 5 (2), 154–168.
- Michalet, X.; Pinaud, F. F.; Bentolila, L. A.; Tsay, J. M.; Doose, S.; Li, J. J.; Sundaresan, G.; Wu, A. M.; Gambhir, S. S.; Weiss, S. *Science* **2005**, 307 (5709), 538–544.
- Park, J.; Joo, J.; Kwon, S. G.; Jang, Y.; Hyeon, T. *Angew. Chem. Int. Ed.* **2007**, 46 (25), 4630–4660.
- Yin, Y.; Alivisatos, A. P. *Nature* **2005**, 437 (7059), 664–670.
- Peng, X. G.; Manna, L.; Yang, W. D.; Wickham, J.; Scher, E.; Kadavanich, A.; Alivisatos, A. P. *Nature* **2000**, 404 (6773), 59–61.
- Yu, H.; Li, J. B.; Loomis, R. A.; Gibbons, P. C.; Wang, L. W.; Buhro, W. E. *J. Am. Chem. Soc.* **2003**, 125 (52), 16168–16169.
- Joo, J.; Son, J. S.; Kwon, S. G.; Yu, J. H.; Hyeon, T. *J. Am. Chem. Soc.* **2006**, 128 (17), 5632–5633.
- Ithurria, S.; Dubertret, B. *J. Am. Chem. Soc.* **2008**, 130 (49), 16504–16505.
- Novoselov, K. S.; Geim, A. K.; Morozov, S. V.; Jiang, D.; Zhang, Y.; Dubonos, S. V.; Grigorieva, I. V.; Firsov, A. A. *Science* **2004**, 306 (5696), 666–669.

- (13) Ithurria, S.; Tessier, M. D.; Mahler, B.; Lobo, R. P.; Dubertret, B.; Efros, A. L. *Nat. Mater.* **2011**, *10* (12), 936–41.
- (14) Huang, M. H.; Cavallo, F.; Liu, F.; Lagally, M. G. *Nanoscale* **2011**, *3* (1), 96–120.
- (15) Son, J. S.; Wen, X. D.; Joo, J.; Chae, J.; Baek, S. I.; Park, K.; Kim, J. H.; An, K.; Yu, J. H.; Kwon, S. G.; Choi, S. H.; Wang, Z. W.; Kim, Y. W.; Kuk, Y.; Hoffmann, R.; Hyeon, T. *Angew. Chem. Int. Ed.* **2009**, *48* (37), 6861–6864.
- (16) Liu, Y. H.; Wayman, V. L.; Gibbons, P. C.; Loomis, R. A.; Buhro, W. E. *Nano Lett.* **2010**, *10* (1), 352–357.
- (17) Liu, Y. H.; Wang, F. D.; Wang, Y. Y.; Gibbons, P. C.; Buhro, W. E. *J. Am. Chem. Soc.* **2011**, *133* (42), 17005–17013.
- (18) Li, Z.; Peng, X. G. *J. Am. Chem. Soc.* **2011**, *133* (17), 6578–6586.
- (19) (a) Ithurria, S.; Talapin, D. V. *J. Am. Chem. Soc.* **2012**, *134* (45), 18585–90. (b) Mahler, B.; Nadal, B.; Bouet, C.; Patriarche, G.; Dubertret, B. *J. Am. Chem. Soc.* **2012**, *134* (45), 18591–8.
- (20) Ithurria, S.; Bousquet, G.; Dubertret, B. *J. Am. Chem. Soc.* **2011**, *133* (9), 3070–3077.
- (21) Bouet, C.; Mahler, B.; Nadal, B.; Abecassis, B.; Tessier, M. D.; Ithurria, S.; Xu, X.; Dubertret, B. *Chem. Mater.* **2013**, *25*, 639–645.
- (22) (a) Li, Z.; Qin, H. Y.; Guzun, D.; Benamara, M.; Salamo, G.; Peng, X. G. *Nano Res.* **2012**, *5* (5), 337–351. (b) Son, J. S.; Park, K.; Kwon, S. G.; Yang, J.; Choi, M. K.; Kim, J.; Yu, J. H.; Joo, J.; Hyeon, T. *Small* **2012**, *8* (15), 2394–2402.
- (23) *Landolt-Bornstein Tables, New Series, Group III: Crystals and Solid State Physics*. Springer-Verlag: Berlin, 1982; Vol. 17, pp 225–229.
- (24) Gur, I.; Fromer, N. A.; Chen, C. P.; Kanaras, A. G.; Alivisatos, A. P. *Nano Lett.* **2007**, *7* (2), 409–414.
- (25) Xie, X.; Kwok, S. Y.; Lu, Z. Z.; Liu, Y. K.; Cao, Y. L.; Luo, L. B.; Zapien, J. A.; Bello, I.; Lee, C. S.; Lee, S. T.; Zhang, W. *Nanoscale* **2012**, *4* (9), 2914–2919.
- (26) Yu, W. W.; Wang, Y. A.; Peng, X. G. *Chem. Mater.* **2003**, *15* (22), 4300–4308.
- (27) Talapin, D. V.; Haubold, S.; Rogach, A. L.; Kornowski, A.; Haase, M.; Weller, H. *J. Phys. Chem. B* **2001**, *105* (12), 2260–2263.
- (28) Mamedova, N. N.; Kotov, N. A.; Rogach, A. L.; Studer, J. *Nano Lett.* **2001**, *1* (6), 281–286.
- (29) Carbone, L.; Kudera, S.; Carlino, E.; Parak, W. J.; Giannini, C.; Cingolani, R.; Manna, L. *J. Am. Chem. Soc.* **2006**, *128* (3), 748–55.
- (30) Sun, J. W.; Buhro, W. E.; Wang, L. W.; Schrier, J. *Nano Lett.* **2008**, *8* (9), 2913–2919.
- (31) Pan, J.; Qian, Y. T. *Mater. Lett.* **2012**, *85*, 132–134.
- (32) Tang, Z. Y.; Zhang, Z. L.; Wang, Y.; Glotzer, S. C.; Kotov, N. A. *Science* **2006**, *314* (5797), 274–278.
- (33) Lhuillier, E.; Keuleyan, S.; Zolotavin, P.; Guyot-Sionnest, P. *Adv. Mater.* **2013**, No. 25, 137–141.
- (34) Als-Nielsen, J.; McMorrow, D. *Elements of Modern X-ray Physics*. 2nd ed.; John Wiley and Sons: New York, 2011.
- (35) Butter, K.; Hoell, A.; Wiedenmann, A.; Petukhov, A. V.; Vroege, G. J. *J. Appl. Crystallogr.* **2004**, *37*, 847–856.
- (36) Leatherdale, C. A.; Woo, W. K.; Mikulec, F. V.; Bawendi, M. G. *J. Phys. Chem. B* **2002**, *106* (31), 7619–7622.
- (37) Shirasaki, Y.; Supran, G. J.; Bawendi, M. G.; Bulovic, V. *Nat. Photonics* **2012**, *7*, 13–23.
- (38) Lee, M. M.; Teuscher, J.; Miyasaka, T.; Murakami, T. N.; Snaith, H. J. *Science* **2012**, *338* (6107), 643–647.
- (39) Sukhovatkin, V.; Hinds, S.; Brzozowski, L.; Sargent, E. H. *Science* **2009**, *324* (5934), 1542–1544.
- (40) Tessier, M. D.; Javaux, C.; Maksimovic, I.; Loriette, V.; Dubertret, B. *ACS Nano* **2012**, *6* (8), 6751–6758.
- (41) Yu, D.; Wang, C. J.; Guyot-Sionnest, P. *Science* **2003**, *300* (5623), 1277–1280.
- (42) Kovalenko, M. V.; Scheele, M.; Talapin, D. V. *Science* **2009**, *324* (5933), 1417–1420.
- (43) Liu, Y.; Gibbs, M.; Perkins, C. L.; Tolentino, J.; Zarghami, M. H.; Bustamante, J.; Law, M. *Nano Lett.* **2011**, *11* (12), 5349–5355.